Nanomechanical Switch Designs to Overcome the Surface Adhesion Energy Limit

I-Ru Chen, *Member, IEEE*, Chuang Qian, Eli Yablonovitch, *Fellow, IEEE*, and Tsu-Jae King Liu, *Fellow, IEEE*

***Abstract*— An analytical model is developed to assess the switching energy of a nanomechanical switch. Alternative switch designs are proposed to leverage spring-restoring force to counterbalance surface adhesion force, reducing the depth of the potential energy well created by contact adhesion and thereby overcoming the surface adhesion energy limit.**

***Index Terms*— Nanomechanical switch, adhesion, effective spring, tunneling.**

I. Introduction

MINIATURE mechanical switches recently have attracted significant attention for future energy-efficient digital logic integrated circuits due to their zero OFF-state leakage and abrupt switching characteristics [1], [2]. Theoretical studies and experimental efforts have been undertaken to investigate nanometer-scale mechanical (nanomechanical) switches driven by electrostatic, piezoelectric, or magnetic forces [3]–[8], because the benefits of miniaturization include lower mechanical delay for faster circuit operation and lower operating voltage for lower switching energy [3], [9]. Since a mechanical switch operates by making and breaking physical contact between conductive electrodes, researchers have studied contact scaling properties and closing/opening dynamics in order to predict its scaling limit [9]–[12]. It is generally believed that contact adhesion sets a lower limit for the switching energy of a mechanical switch [9], [10], [12]. In this letter, we propose compact ($< 1\ \mu m^2$ footprint), low-voltage (< 0.1 V) nanomechanical switch designs that can overcome the contact adhesion switching energy limit, paving a pathway to ultimately energy-efficient nanomechanical switches.

II. Analysis of Conventional Switch Design

In general, three types of force affect a nanomechanical switch: an applied force that actuates the suspended structure, surface adhesive force (F_{adh}) at the physical contact(s), and the spring restoring force (F_{spring}) of the suspended structure. The governing equations for these forces and their corresponding potential energies are modeled to assess the energy efficiency of nanomechanical switches of various designs. Although electrostatic force (F_{elec}) is assumed herein to be the actuation mechanism, the switch model can be easily adapted by replacing the electrostatic force equation.

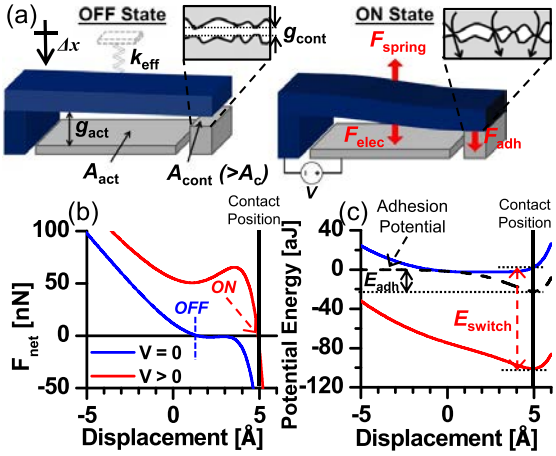

Fig. 1. Conventional nanomechanical switch: (a) Isometric views in OFF and ON states, showing key dimensions and relevant forces exerted on the movable structure. The magnified view of the contacts indicates that only a few asperities are in physical contact at ON state due to surface roughness. (b) Net force (F_{net}) *vs.* displacement (Δx) curves. (c) Potential energy profiles showing minima at $\Delta x \sim 0$ Å for OFF state and $\Delta x = 5$ Å (in contact) for ON state ($V = 0.2$ V). The energy required to operate this switch is $E_{switch} = 102.44$ aJ.

Fig. 1(a) illustrates the operation of a conventional three-terminal mechanical switch design, showing the relevant forces and geometrical design parameters. In the OFF state, a contact air gap separates the movable suspended electrode (which has an effective spring constant k_{eff}) from the fixed contacting electrode. When a sufficiently large voltage is applied between the suspended electrode and the actuator electrode ($V > 0$), $F_{elec} \geq F_{spring}$ such that the suspended electrode comes into contact with the contacting electrode so that the switch is turned ON. To turn OFF the switch, the applied voltage is removed ($V = 0$) and $F_{spring} > F_{adh}$ is required to break the contact. This means that F_{elec} must be greater than F_{adh}, and therefore contact adhesion sets a lower limit for the switching energy [9], [10]. Note that, as fabricated ($V = 0$), the actuation gap and area are larger than the contact gap and area, respectively (*i.e.* $g_{act} > g_{cont}$ and $A_{act} > A_{cont}$), for robust low-voltage operation [13].

F_{elec} and F_{spring} and their corresponding potential energies E_{elec} and E_{spring} are analytically modeled assuming a parallel-plate actuator and linear spring (Hooke's law):

$$F_{elec} = \frac{\varepsilon_0 A_{act} V^2}{2 d_{act}^2} \quad \text{and} \quad E_{elec} = -\frac{\varepsilon_0 A_{act} V^2}{2 d_{act}};$$

$$F_{spring} = -k_{eff}\,\Delta x \quad \text{and} \quad E_{spring} = \frac{1}{2} k_{eff}\,(\Delta x)^2,$$

Manuscript received April 30, 2015; revised July 24, 2015; accepted July 27, 2015. Date of publication July 30, 2015; date of current version August 21, 2015. This work was supported by the National Science Foundation (NSF) Center for Energy Efficient Electronics Science under Award 0939514. The work of I.-R. Chen was supported by the NSF Graduate Research Fellowship Program. The review of this letter was arranged by Editor M. Tabib-Azar.

The authors are with the Department of Electrical Engineering and Computer Sciences, University of California at Berkeley, Berkeley, CA 94720 USA (e-mail: iruchen@eecs.berkeley.edu).

Color versions of one or more of the figures in this letter are available online at http://ieeexplore.ieee.org.

Digital Object Identifier 10.1109/LED.2015.2463119

where ε_0 is the permittivity of air, d_{act} is the distance between the actuator and suspended electrodes, d_{cont} is the distance between the contacting electrodes, and Δx is the displacement of the suspended electrode. For the conventional switch design, $d_{cont} = D_0 + g_{cont} - \Delta x$ and $d_{act} = D_0 + g_{act} - \Delta x$.

Due to surface roughness, the real contact area (A_c) usually is a small fraction of the apparent contact area, and only A_c is assumed to be relevant for surface energy calculations [14]. F_{adh} includes van der Waals force, capillary force, and material bonding [10], [11]. For a metal-to-metal contact, which is desirable for low ON-state resistance, the metallic bonding force originating from electron interaction is dominant [9], [15]. The surface energy and force between metal interfaces can be modeled using the following universal relationship [16], [17]:

$$E_{adh}(d_{cont}) = -2\gamma A_c\left(1 + \frac{d_{cont} - D_0}{\lambda_M}\right)e^{-\frac{d_{cont}-D_0}{\lambda_M}} \quad \text{and}$$

$$F_{adh}(d_{cont}) = 2\gamma A_c\left(\frac{d_{cont} - D_0}{\lambda_M^2}\right)e^{-\frac{d_{cont}-D_0}{\lambda_M}},$$

where γ is the surface energy density, D_0 is the average atomic distance between two perfectly smooth surfaces in contact, and λ_M is a characteristic decay length related to the Thomas-Fermi screening length [16]. E_{adh} and F_{adh} expressions above also include repulsive force between atoms. A universal value of $D_0 = 0.165$ nm well predicts E_{adh} between two solid surfaces [18]. λ_M is typically 0.5-1.5 Å [17], but is larger for a confined contact volume due to reduced electron density [19].

The energy required to separate two metal surfaces in contact is $E_{adh}(\infty) - E_{adh}(D_0) = 2\gamma A_c$, which is 22 aJ for gold (Au) contacting electrodes with $A_c = 10$ nm^2, $\gamma = 1.1$ J/m^2 and $\lambda_M = 1.2$ Å [20]. The proposed model can be adapted for other contacting metals, which generally have similar γ and λ_M. Surface oxidation and material transfer are assumed to be negligible during switching, so that the properties of the contacting surfaces (A_c, γ, λ_M) are constant.

Fig. 1(b) shows how the net force on the suspended electrode ($F_{net} = F_{spring} + F_{elec} + F_{adh}$) depends on Δx, while Fig. 1(c) shows the corresponding potential energy (E) plot. When a sufficiently large actuation voltage is applied, $F_{net} > 0$ for all $\Delta x < g_{cont}$ so that the suspended electrode moves into contact with the contacting electrode. When no voltage is applied, F_{spring} restores the suspended actuator back to $\Delta x \sim 1$ Å (non-zero due to F_{adh}), corresponding to the stable operating point where $F_{net} = 0$ and $dF_{net}/d(\Delta x) < 0$. Local energy minima are observed at the stable operating points. The geometric, material, and electrical parameter values used to arrive at the modeling results in Fig. 1(b) and 1(c) are summarized in Table I. The aggressively scaled g_{cont} (similar to lattice constant of Au, $a_{Au} = 4.065$ Å) is beneficial since F_{adh} reduces required F_{elec} and thus required actuation voltage. The energy required to operate the switch (E_{switch}) is the electrostatic energy stored in the actuation air-gap capacitor when voltage is applied, as indicated on Fig. 1(c). The minimum energy required to operate a conventional nano-electro-mechanical switch is four times the contact adhesion energy [3], which is $4 \times 2\gamma A_c = 88$ aJ for the contact model parameter values used in this letter.

TABLE I
MODELING PARAMETERS AND RESULTS

Symbol	Description	Unit	Conventional (Sec. II)	Tunneling (Sec. III-A)	Bistable Tunneling (Sec. III-B)
A_{act}	Actuation area	μm^2	0.7	0.7	0.16
A_c	Real contact area	nm^2	10		
g_{act}	Fabricated actuation gap	Å	17		
g_{cont}	Fabricated contact gap	Å	5		
k_{eff}	Effective spring constant	N/m	195	172	182
γ	Surface energy density	J/m^2	1.1		
λ_M	Characteristic decay length	Å	1.2		
V	Switching voltage	V	0.2	0.1	0.1
E_{switch}	Total energy consumed during one switching cycle	aJ	102.44	18.12	7.61
E_{limit}	Switching energy limit for a conventional switch	aJ	88		

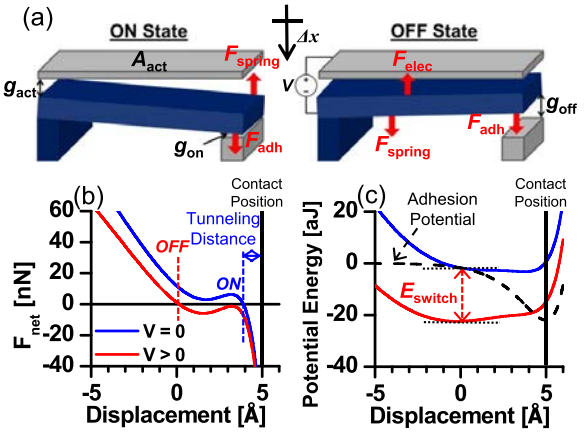

Fig. 2. Tunneling nanomechanical switch: (a) Isometric views in ON and OFF states. (b) Force *vs.* displacement curves. (c) Potential energy profiles showing minima at $\Delta x \sim 0$ Å for OFF state (V > 0) and $\Delta x \sim 4$ Å (near contact) for ON state (V > 0).

III. PROPOSED NEW SWITCH DESIGNS

A. Nanomechanical Tunneling Switch

Fig. 2(a) illustrates the operation of a proposed new tunneling switch design in which the actuator electrode and contacting electrode are located on opposite sides of the suspended electrode. The movable electrode has lower k_{eff} (172 N/m) so that F_{adh} actuates it into the ON state without an applied voltage; F_{adh} and F_{spring} reach a balance within 1 Å of contact to allow for significant electron conduction via tunneling. To turn OFF the switch, electrostatic force is applied to actuate the suspended electrode away from the contacting electrode and thereby reduce the tunneling current. Since F_{elec} and F_{spring} work together to counterbalance F_{adh}, less electrostatic force is needed to operate the switch.

Figs. 2(b) and 2(c) show the net force ($F_{spring} - F_{elec} + F_{adh}$) and potential energy plots for the tunneling switch design, respectively. For the purpose of comparison, the actuation and contact design parameters (γ, λ_M, g_{cont}, g_{act}, A_c, and A_{act}) of this tunneling switch are taken to be identical to those

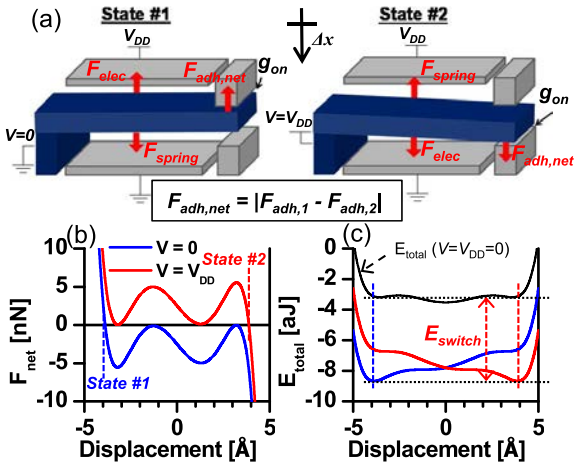

Fig. 3. Complementary tunneling switch design: (a) Isometric views in the two complementary states. (b) Force-*vs.*-Δx curves. (c) Potential energy profiles showing minima near $\Delta x = -5$Å and 5Å for the two states.

of the conventional switch design in the previous section. Stable operating points and energy minima are found near contact ($\Delta x \sim g_{\text{cont}} - 1$Å) with zero applied voltage, and near $\Delta x = 0$ with a small applied voltage (0.1 V). The energy required to operate this switch ($E_{\text{switch}} = 18.12$ aJ) is lower than the adhesion energy because the spring restoring force effectively reduces the depth of the potential well due to adhesive force (depicted by the dashed line in Fig. 2(c)) and prevents the suspended electrode from touching the contacting electrode (*i.e.* $\Delta x < g_{\text{cont}}$). The tradeoff is increased ON-state resistance due to the tunneling conduction mechanism. The tunneling current across an air gap is given by the equation $I_{\text{tunnel}} = CAVe^{-ad_{\text{cont}}\sqrt{B}}$, where $C \cong 3.16\times10^{13}$ A/m^2/V, A is the tunneling area, V is the contact voltage, $a = 10.25$ nm^{-1}, and B is the average barrier height for an electron at the Fermi energy [21]. As a lower-bound $A = A_c = 10$ nm^2 and $B = 4.28$ eV for Al so that $R_{\text{ON}} \equiv V/I_{\text{tunnel}} \cong 26.4$ kΩ. For comparison, R_{ON} is typically ∼1 kΩ for a nanoscale metal-to-metal contact. The small displacement (∼4Å) yields an ON/OFF current ratio of $\sim10^4$.

B. Bistable Nanomechanical Tunneling Switch

Fig. 3 illustrates the operation and force/energy modeling results for a bistable switch design with actuator and contacting electrodes located on both sides of the suspended electrode. The actuator electrodes are biased at the supply voltage (V_{DD}) and ground, so that electrostatic force actuates the suspended structure from one contacting electrode to the other as the voltage applied to the suspended electrode is varied from ground to V_{DD}. Again, to allow a fair comparison, the actuation and contact design parameters (γ, λ_M, g_{cont}, g_{act}, A_c, and A_{act}) for this switch design are taken to be identical to those of the conventional switch design in the previous section. The energy required to switch between the two states (E_{switch}) is 7.61 aJ, significantly lower than the $4 \times 2\gamma A_c$ limit (88 aJ) due to the reduced potential well depth and non-contact operation.

IV. Conclusion

The surface adhesion energy limit for a nanomechanical switch can be overcome by designing it to be normally ON so that spring restoring force reduces the actuation force required for switching. The tradeoff for this tunneling-mode design is larger ON-state resistance (on the order of 10 kΩ) and reduced ON/OFF current ratio ($\sim10^4$). The normally ON design can be leveraged to achieve a bistable switch which can be attractive for memory and non-volatile logic applications [22].

References

[1] M. Spencer *et al.*, "Demonstration of integrated mico-electro-mechanical switch circuits for VLSI applications," *IEEE J. Solid-State Circuits*, vol. 46, no. 1, pp. 308–320, Jan. 2011.
[2] S. Han *et al.*, "Ultra-low power NEMS FPGA," in *Proc. Int. Conf. Comput.-Aided Design. ACM ICCAD*, 2012, pp. 533–538.
[3] H. Kam *et al.*, "Design, optimization, and scaling of MEM relays for ultra-low-power digital logic," *IEEE Trans. Electron Devices*, vol. 58, no. 1, pp. 236–250, Jan. 2011.
[4] W. W. Jang *et al.*, "Fabrication and characterization of a nanoelectromechanical switch with 15-nm-thick suspension air gap," *Appl. Phys. Lett.*, vol. 92, no. 10, p. 103110, Mar. 2008.
[5] S. Chong *et al.*, "Integration of nanoelectromechanical relays with silicon nMOS," *IEEE Trans. Electron Devices*, vol. 59, no. 1, pp. 255–258, Jan. 2012.
[6] T. He *et al.*, "Silicon carbide (SiC) nanoelectromechanical switches and logic gates with long cycles and robust performance in ambient air and at high temperature," in *IEDM Tech. Dig.*, Dec. 2013, pp. 4.6.1–4.6.4.
[7] U. Zaghloul, and G. Piazza, "Sub-1-volt piezoelectric nanoelectromechanical relays with millivolt switching capability," *IEEE Electron Device Lett.*, vol. 35, no. 6, pp. 669–671, Jun. 2014.
[8] D. Niarchos, "Magnetic MEMS: Key issues and some applications," *Sens. Actuators A, Phys.*, vol. 109, nos. 1–2, pp. 166–173, Dec. 2003.
[9] C. Pawashe, K. Lin, and K. Kuhn, "Scaling limits of electrostatic nanorelays," *IEEE Trans. Electron Devices*, vol. 60, no. 9, pp. 2936–2942, Sep. 2013.
[10] J. Yaung, L. Hutin, J. Jeon, and T.-J. K. Liu, "Adhesive force characterization for MEM logic relays with sub-micron contacting regions," *J. Microelectromech. Syst.*, vol. 23, no. 1, pp. 198–203, Feb. 2014.
[11] B. Jensen *et al.*, "Adhesion effects on contact opening dynamics in micromachined switches," *J. Appl. Phys.*, vol. 97, no. 10, p. 103535, May 2005.
[12] A. Knoll *et al.*, "Fundamental scaling properties of electro-mechanical switches," *New J. Phys.*, vol. 14, p. 123007, Dec. 2012.
[13] F. Chen *et al.*, "Integrated circuit design with NEM relays," in *Proc. IEEE/ACM Int. Conf. Comput.-Aided Design*, Nov. 2008, pp. 750–757.
[14] B. N. J. Persson, "Contact mechanics for randomly rough surfaces," *Surf. Sci. Rep.*, vol. 61, no. 4, pp. 201–227, Jun. 2006.
[15] A. Banerjea, J. Ferrante, and J. R. Smith, "Adhesion at metal interfaces," in *Fundamentals of Adhesion*, L.-H. Lee, Ed. New York, NY, USA: Plenum, 1991, pp. 325–348.
[16] J. H. Rose, J. Ferrante, and J. R. Smith, "Universal binding energy curves for metals and bimetallic interfaces," *Phys. Rev. Lett.*, vol. 47, no. 9, pp. 675–678, Aug. 1981.
[17] J. H. Rose, J. Ferrante, and J. R. Smith, "Universal features of bonding in metals," *Phys. Rev. B*, vol. 28, pp. 1835–1845, Aug. 1983.
[18] J. Israelachvili, *Intermolecular and Surface Forces*, 3rd. ed. New York, NY, USA: Academic, 2011, pp. 253–289.
[19] A. Schirmeisen *et al.*, "Metallic adhesion and tunnelling at the atomic scale," *New J. Phys.*, vol. 2, no. 1, pp. 29.1–29.10, 2000.
[20] J. Cognard, "Adhesion to gold: A review," *Gold Bull.*, vol. 17, no. 4, pp. 131–139, 1984.
[21] E. C. Teague, "Room temperature gold-vacuum-gold tunneling experiments," *J. Res. Nat. Bur. Stand.*, vol. 91, no. 4, pp. 171–233, 1986.
[22] N. Xu *et al.*, "Hybrid CMOS/BEOL-NEMS technology for ultra-low-power IC applications," in *IEDM Tech. Dig.*, Dec. 2014, pp. 28.8.1–28.8.4.